

Van der Waals density-functional theory study for bulk solids with BCC, FCC, and diamond structures

Jinwoo Park^a, Byung Deok Yu^{b,*}, Suklyun Hong^{a,*}

^a*Graphene Research Institute and Department of Physics, Sejong University, Seoul 143-747, Republic of Korea*

^b*Department of Physics, University of Seoul, Seoul 130-743, Republic of Korea*

Abstract

Proper inclusion of van der Waals (vdW) interactions in theoretical simulations based on standard density functional theory (DFT) is crucial to describe the physics and chemistry of systems such as organic and layered materials. Many encouraging approaches have been proposed to combine vdW interactions with standard approximate DFT calculations. Despite many vdW studies, there is no consensus on the reliability of vdW methods. To help further development of vdW methods, we have assessed various vdW functionals through the calculation of structural properties at equilibrium, such as lattice constants, bulk moduli, and cohesive energies, for bulk solids, including alkali, alkali-earth, and transition metals, with BCC, FCC, and diamond structures as the ground state structure. These results provide important information for the vdW-related materials research, which is essential for designing and optimizing materials systems for desired physical and chemical properties.

Keywords: Van der Waals interactions, Density functional theory, Bulk solids, Lattice constant, Bulk modulus, Cohesive energy

1. Introduction

The development of approximate density functional theory (DFT) [1, 2] methods that are able to account for van der Waals (vdW) interactions has attracted a great deal of interest due to its importance in the theoretical description of organic or layered materials as well as that of physical, chemical, and biological processes [3–9]. Many encouraging schemes and algorithms have been proposed to include vdW interactions in theoretical simulations based on standard DFT. One of the promising vdW approaches is the vdW density functional (vdW-DF) method, which does not depend on external input parameters and is based directly on the electron density [10]. In the vdW-DF method, the exchange-correlation (XC) energy is given as

$$E_{\text{XC}} = E_{\text{X}}^{\text{GGA}} + E_{\text{C}}^{\text{LDA}} + E_{\text{C}}^{\text{nl}}, \quad (1)$$

where $E_{\text{X}}^{\text{GGA}}$ is the generalized gradient approximation (GGA) to the exchange energy, $E_{\text{C}}^{\text{LDA}}$ is the local density approximation (LDA) to the correlation energy, and E_{C}^{nl} is the nonlocal electron correlation energy. In the case of the vdW-DF approach, the computational time increases by 50% compared to standard DFT calculations such as the LDA and the GGA calculations [11]. Depending on the selection of the exchange functional, there are many vdW-DF methods. Here we consider the five vdW-DF functionals; revPBE-vdW [10], rPW86-vdW2 [12, 13], optPBE-vdW [14], optB88-vdW [14], and optB86b-vdW [15]. In addition, there is another widely used vdW approach, the so-called dispersion-corrected DFT-D in which an atom-pairwise potential is added to a standard DFT result. In the original DFT-D scheme [16], the predetermined constant dispersion coefficients are assigned to an element irrespective of its environment. To improve this, the dispersion coefficients are further modified to vary with the environment of an element. In contrast to the vdW-DF schemes, the DFT-D schemes do not add a significant computational cost

*Corresponding authors

Email addresses: ybd@uos.ac.kr (Byung Deok Yu), hong@sejong.ac.kr (Suklyun Hong)

compared to the standard DFT calculations. In the DFT-D schemes, we consider the five vdW functionals; DFT-D2 [17], DFT-D3 [18], DFT-D3(BJ) [19], DFT-TS [20], and DFT-TS-SCS [21, 22]. The environment-dependent DFT-D3 scheme has zero damping for small interatomic distances, whereas the DFT-D3(BJ) scheme has rational damping to finite values (BJ-damping) as Becke and Johnson proposed. Grimme *et al.* suggested that the DFT-D3(BJ) performed slightly better than the DFT-D3 for noncovalently-bonded materials systems [19]. In the DFT-TS scheme, the dispersion coefficients are determined by employing the partitioning of the electron density [20]. The DFT-TS scheme can be further modified by incorporating self-consistent long-range screening effects [21, 22]. This modified scheme is herein called the DFT-TS-SCS functional. Tkatchenko *et al.* report that the DFT-TS-SCS functional performs better than the DFT-TS functional [21, 22]. However, despite many vdW studies, the assessment of the performance of the vdW functionals on a broad range of material systems is lacking.

In the present work, we have investigated structural properties (lattice constants, bulk moduli, and cohesive energies) at equilibrium for bulk solids with body centered cubic (BCC), face centered cubic (FCC), and diamond (DIA) structures, to assess the performance of various vdW functionals based on the DFT. We herein consider the ten vdW functionals implemented in the Vienna *Ab-initio* Simulation Package (VASP) code [23–26]; revPBE-vdW, rPW86-vdW2, optPBE-vdW, optB88-vdW, optB86b-vdW, DFT-D2, DFT-D3, DFT-D3(BJ), DFT-TS, and DFT-TS-SCS functionals. For comparison, the LDA and GGA calculations were also performed. Our calculations show that the five vdW functionals of optB86b-vdW, optB88-vdW, optPBE-vdW, DFT-D3, and DFT-D3(BJ) give better performance compared to the other vdW functionals. Differences among the results from the five vdW functionals are also discussed. These results provide important information for further development of vdW methods to improve the description of a wide range of materials systems.

The paper is organized as follows. In Sec. 2, the computational method and settings used in this study are briefly described. The results and discussion are presented in Sec. 3. Finally, the conclusions are stated in Sec. 4.

2. Computation method

We employed the VASP code to perform the DFT calculations, including spin effects for magnetic elements, with various vdW functionals [23–26]. In this work, we considered ten vdW functionals implemented in the VASP; revPBE-vdW [10], rPW86-vdW2 [12, 13], optPBE-vdW [14], optB88-vdW [14], optB86b-vdW [15], DFT-D2 [17], DFT-D3 [18], DFT-D3(BJ) of Becke-Jonson [19], DFT-TS [20], and DFT-TS-SCS [21, 22]. For comparison, LDA and GGA calculations were also performed using the Ceperley-Alder [27] and the Perdew-Burke-Ernzerhof (PBE) [28] expressions, respectively, for the exchange-correlation functional. In the case of the DFT-D schemes [DFT-D2, DFT-D3, DFT-D3(BJ), DFT-TS, and DFT-TS-SCS], we used the PBE parameterization of the GGA for the exchange-correlational functional. For electron-ion interactions, the projector augmented-wave (PAW) method [29, 30] was used. We considered 29 elements with BCC, FCC, and diamond structures as the ground state in the bulk phase. In the calculations, the electronic wave functions were expanded by plane waves with an energy cutoff of 700 eV. The \mathbf{k} -space integration was performed using a Γ -centered $12 \times 12 \times 12$ mesh in the Brillouin zone (BZ) of the primitive cell. The tetrahedron method with Blöchl corrections [31, 32] was used to improve the computational convergence. We performed total energy calculations to obtain the ground state properties such as the equilibrium lattice constant, the bulk modulus, and the cohesive (atomization) energy. The ground state properties were determined by fitting the calculated total energy as a function of the volume to the Birch-Murnaghan equation of state [33–35]. In the fitting, a set of eleven different volumes around the experimental equilibrium volume corresponding to the equilibrium lattice constant was used.

3. Results and discussion

3.1. Lattice constant

The equilibrium lattice constants calculated with the ten vdW functionals are summarized in Table 1, and the relative errors in the equilibrium lattice constants with respect to the experimental values are shown in Fig. 1. For comparison, we also present the results of the standard DFT functionals of LDA and GGA. The standard GGA functional gives the relative errors in the range of $\pm 2\%$, while the standard DFT functional of LDA shows shorter equilibrium lattice constants than those from the other functionals, indicating the well known overbinding of atoms in

Table 1: Equilibrium lattice constants (in Å) for bulk solids with BCC, FCC, and diamond (DIA) structures using the ten vdW functionals. In addition, standard DFT calculation results using LDA and GGA are also shown. The experimental lattice constants [36] are measured at finite temperatures, in contrast to the theoretical lattice constants obtained from ground-state electronic structure calculations at zero temperature. For comparison, the experimental values were corrected to the $T = 0$ limit using thermal expansion corrections [37] for the solids (denoted with an asterisk) whose zero-point anharmonic expansion values are available.

Solid	Crystal structure	revPBE vdW	rPW86 vdW2	optB86b vdW	optB88 vdW	optPBE vdW	DFT D2	DFT D3	DFT D3(BJ)	DFT TS	DFT TS-SCS	PAW LDA	PAW GGA	Expt.
Li	BCC	3.453	3.393	3.457	3.435	3.442	3.270	3.374	3.329	2.607	3.122	3.367	3.439	3.449*
C	DIA	3.599	3.605	3.570	3.575	3.584	3.564	3.565	3.558	3.553	3.564	3.535	3.573	3.543*
Na	BCC	4.214	4.135	4.176	4.152	4.178	3.980	4.161	4.078	4.131	3.852	4.055	4.193	4.210*
Al	FCC	4.084	4.087	4.034	4.054	4.058	4.010	4.007	3.982	3.921	4.002	3.984	4.040	4.020*
Si	DIA	5.513	5.540	5.456	5.469	5.484	5.412	5.453	5.420	5.446	5.438	5.403	5.469	5.416*
K	BCC	5.289	5.174	5.198	5.162	5.222	5.156	5.226	5.163	4.345	4.943	5.043	5.284	5.212*
Ca	FCC	5.553	5.493	5.464	5.450	5.501	5.381	5.498	5.441	5.169	5.301	5.338	5.532	5.553*
V	BCC	3.007	3.026	2.958	2.969	2.982	2.970	2.938	2.932	2.917	2.954	2.912	2.978	3.030
Cr	BCC	2.866	2.887	2.821	2.833	2.843	2.815	2.809	2.809	2.770	2.808	2.779	2.836	2.880
Fe	BCC	2.873	2.889	2.806	2.821	2.838	2.802	2.805	2.806	2.779	2.812	2.749	2.832	2.870
Ni	FCC	3.572	3.609	3.488	3.511	3.529	3.459	3.476	3.477	3.424	3.489	3.422	3.518	3.520
Cu	FCC	3.705	3.750	3.601	3.629	3.651	3.571	3.568	3.568	3.547	3.607	3.524	3.635	3.595*
Ge	DIA	5.895	5.973	5.764	5.798	5.828	5.666	5.760	5.723	5.749	5.730	5.647	5.783	5.640*
Rb	BCC	5.666	5.545	5.535	5.501	5.578	5.443	5.615	5.551	5.666	5.374	5.668	5.576*	
Sr	FCC	6.057	6.004	5.921	5.911	5.980	5.760	5.985	5.924	6.306	5.731	5.788	6.026	6.045*
Nb	BCC	3.340	3.377	3.288	3.303	3.314	3.308	3.265	3.264	3.214	3.269	3.247	3.308	3.300
Mo	BCC	3.183	3.219	3.139	3.154	3.161	3.145	3.124	3.122	3.084	3.123	3.106	3.151	3.150
Rh	FCC	3.879	3.942	3.803	3.829	3.841	3.773	3.786	3.788	3.767	3.806	3.752	3.824	3.793*
Pd	FCC	4.012	4.083	3.905	3.938	3.957	3.888	3.886	3.889	3.912	3.921	3.841	3.942	3.875*
Ag	FCC	4.242	4.313	4.091	4.130	4.163	4.131	4.073	4.072	4.068	4.117	4.003	4.147	4.056*
Sn	DIA	6.764	6.876	6.593	6.637	6.677	6.505	6.612	6.571	6.538	6.577	6.478	6.652	6.490
Cs	BCC	6.134	5.989	5.942	5.899	6.014	4.235	6.111	6.039	4.382	5.809	5.760	6.161	6.039*
Ba	BCC	5.073	5.057	4.904	4.915	4.986	4.203	4.974	4.935	5.021	4.724	4.768	5.030	4.995*
Ta	BCC	3.340	3.375	3.292	3.306	3.317	3.260	3.273	3.276	3.235	3.281	3.248	3.309	3.300
W	BCC	3.203	3.239	3.163	3.178	3.184	3.106	3.147	3.148	3.123	3.154	3.129	3.172	3.160
Ir	FCC	3.923	3.986	3.861	3.886	3.892	3.767	3.838	3.843	3.844	3.862	3.819	3.873	3.840
Pt	FCC	4.032	4.110	3.949	3.980	3.990	3.839	3.918	3.926	3.934	3.952	3.897	3.968	3.920
Au	FCC	4.245	4.338	4.122	4.161	4.181	3.996	4.099	4.101	4.113	4.134	4.052	4.157	4.080
Pb	FCC	5.134	5.233	4.972	5.018	5.053	5.072	4.971	4.948	4.949	4.997	4.875	5.031	4.902*

the LDA approach [38, 39]. In the case of the vdW functionals, optB86b-vdW, optB88-vdW, optPBE-vdW, and DFT-D3 show the relative errors in the range of $\pm 3\%$. The DFT-D3(BJ) functional shows the relative errors in the range from -3% to $+1\%$ for all elements except for Li. The DFT-TS and DFT-TS-SCS functionals give results comparable to the other vdW functionals, except for the alkali (Li, Na, K, Cs) and alkali-earth (Ca, Sr, Ba) metals. For these two vdW functionals, the DFT-TS-SCS scheme with the self-consistent screening (SCS) effects shows better performance than the DFT-TS scheme without the SCS effects [21, 22]. In the case of revPBE-vdW and rPW86-vdW2, the relative errors range from -3% to $+6\%$. The relative errors are observed to be more scattered compared to those from the vdW functionals of optPBE-vdW, optB88-vdW, optB86b-vdW, DFT-D3, and DFT-D3(BJ). This behavior becomes more significant with the increase of the atomic number.

To further aid our understanding, we discuss the differences among the five vdW results of optPBE-vdW, optB88-vdW, optB86b-vdW, DFT-D3, and DFT-D3(BJ). In the case of DFT-D3, and DFT-D3(BJ), Grimme *et al.* [19] reported that the DFT-D3(BJ) vdW functional with rational damping to finite values for small interatomic distances performed slightly better than the DFT-D3 functional with zero damping when used for noncovalently-bonded systems. Our calculations show that both schemes give very similar results (see Fig. 2). For alkali and alkali-earth metals, however, the DFT-D3 functional gives much better performance than the DFT-D3(BJ) functional (see Fig. 2). In the case of the vdW-DF functionals of optPBE-vdW, optB88-vdW, and optB86b-vdW, the optB86b-vdW functional gives either better or comparable performance in equilibrium lattice constants compared to the optPBE-vdW and optB88-vdW functionals (see Fig. 2).

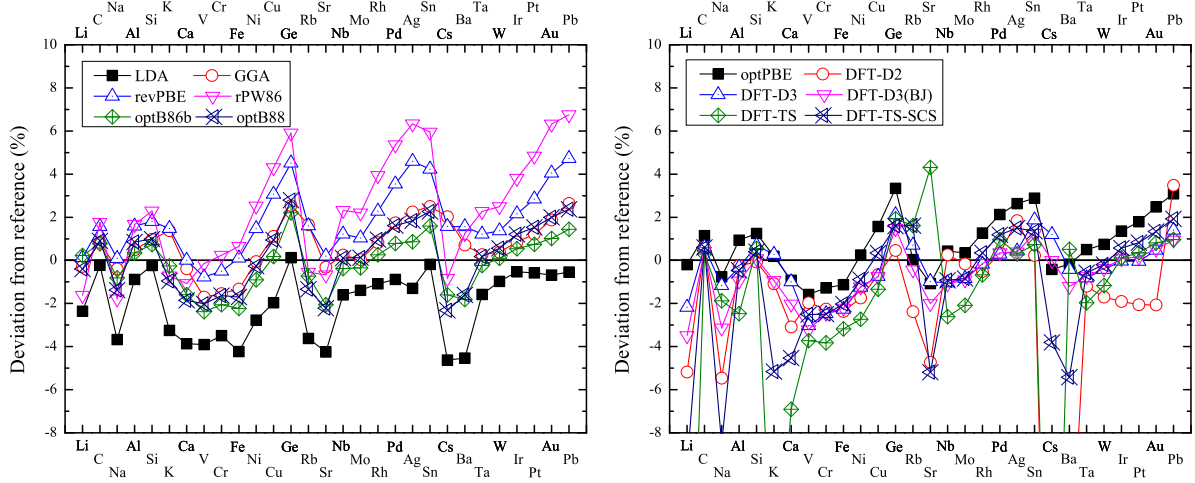


Figure 1: Relative errors in the calculated equilibrium lattice constants with respect to the experimental values. Results are shown for the ten vdW functionals and the standard DFT functionals of LDA and GGA. The positive (negative) values in the relative errors represent the larger (smaller) lattice constants than the experimental values.

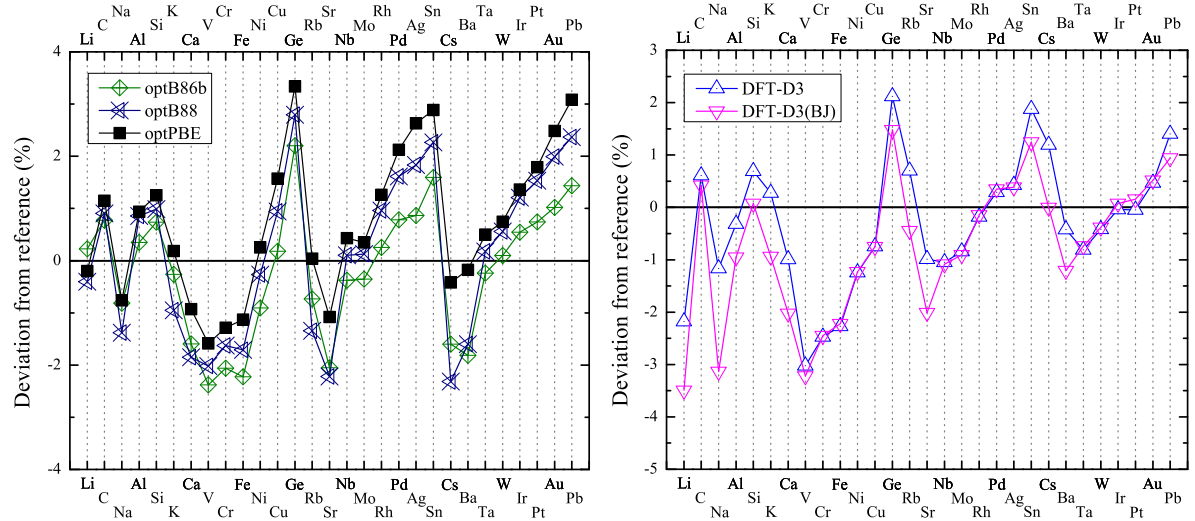


Figure 2: Comparison of the relative errors in the calculated equilibrium lattice constants with respect to the experimental values.

3.2. Bulk modulus

The bulk moduli calculated with the ten vdW functionals are presented in Table 2, and the relative errors in the calculated bulk moduli with respect to the experimental values are shown in Fig. 3. In general, the trend of the bulk moduli is adequately reflected in the behavior of equilibrium lattice constants. Fig. 3 clearly shows that the smaller equilibrium lattice constants lead to larger values of bulk moduli. As expected in the calculated equilibrium lattice constants, the DFT-TS and DFT-TS-SCS vdW functionals show worse results for alkali metals (Li, Na, K, Cs), and the DFT-D2 functional gives a relative error even over 100% for Cs and Ba. In the case of the vdW-DF methods, for most of elements considered herein, the revPBE-vdW and rPW86-vdW give worse results than the other vdW-DF functionals (optB86b-vdW, optB88-vdW, and optPBE-vdW).

Table 2: Bulk moduli (in GPa) for bulk solids with BCC, FCC, and diamond (DIA) structures using the ten vdW functionals. In addition, standard DFT calculation results using LDA and GGA are also shown. The theoretical values are compared to the experimental data. The experimental bulk moduli [36] were corrected to the $T = 0$ limit using thermal effects and zero-point phonon effects (ZPPE) [37] for the solids (denoted with an asterisk) whose ZPPE values are available.

Solid	Crystal structure	revPBE vdW	rPW86 vdW	optB86b vdW	optB88 vdW	optPBE vdW	DFT D2	DFT D3	DFT D3(BJ)	DFT TS	DFT TS-SCS	PAW LDA	PAW GGA	Expt.
Li	BCC	13.694	14.724	13.365	13.748	13.845	14.315	13.513	15.596	187.631	24.117	15.108	13.885	13.3*
C	DIA	404.522	396.193	432.393	426.121	418.944	437.501	433.770	439.529	439.442	434.991	463.489	430.649	443.0
Na	BCC	7.558	8.230	7.845	8.039	7.917	8.621	8.244	8.975	14.229	14.219	9.240	7.826	7.5*
Al	FCC	63.500	57.305	75.135	67.233	69.153	68.368	81.233	85.247	100.028	83.527	82.568	76.049	79.4*
Si	DIA	81.566	76.461	89.842	87.250	85.647	96.468	88.212	91.276	90.158	93.356	95.410	87.711	98.8
K	BCC	3.558	3.947	3.784	3.936	3.787	3.761	4.320	4.132	70.613	5.463	4.470	3.567	3.7*
Ca	FCC	16.444	16.833	17.489	17.138	17.098	17.105	15.826	17.963	15.586	20.594	18.463	17.086	18.4*
V	BCC	172.466	169.806	194.718	188.971	183.512	173.953	203.049	202.604	235.407	198.016	213.713	185.675	161.9
Cr	BCC	237.579	229.519	272.448	262.464	254.717	249.959	279.851	277.020	315.618	283.531	303.323	259.661	190.1
Fe	BCC	147.968	154.123	202.889	192.267	176.236	177.166	213.305	197.352	242.121	194.995	247.046	174.999	168.3
Ni	FCC	165.299	152.039	208.651	196.380	186.375	216.252	207.194	208.723	271.665	211.216	249.627	193.570	186.0
Cu	FCC	110.549	99.879	147.659	137.055	128.539	146.506	159.282	161.663	168.634	148.152	182.498	136.340	137.0
Ge	DIA	48.428	41.953	60.226	56.816	54.096	68.543	59.596	62.472	64.857	65.049	71.363	58.379	77.2
Rb	BCC	2.812	3.119	3.060	3.192	3.028	3.004	3.308	3.143	2.772	2.772	3.570	2.770	2.9*
Sr	FCC	11.014	12.123	12.461	12.744	11.840	12.945	10.281	12.195	13.501	16.295	14.315	11.312	12.4*
Nb	BCC	159.232	153.666	176.423	171.920	167.693	166.781	180.698	180.745	210.983	183.804	189.481	169.206	170.2
Mo	BCC	244.495	227.582	276.592	265.651	259.989	251.293	283.879	283.494	329.543	288.041	299.116	265.888	272.5
Rh	FCC	219.171	191.033	273.980	255.757	245.384	267.614	279.428	279.135	289.154	268.524	314.511	254.550	270.4
Pd	FCC	133.434	116.972	183.377	168.781	157.180	162.033	187.936	187.733	177.399	173.192	222.962	162.581	180.8
Ag	FCC	68.730	61.864	105.174	95.643	85.884	64.765	103.017	108.873	111.938	96.729	135.435	88.903	100.7
Sn	DIA	30.578	26.675	38.707	36.573	34.487	39.692	38.626	39.488	44.543	39.704	44.872	35.827	53.0
Cs	BCC	2.019	2.268	2.173	2.294	2.167	79.424	2.254	2.128	82.969	2.921	2.458	1.937	2.1*
Ba	BCC	8.906	9.597	9.595	9.933	9.349	84.987	8.264	9.097	9.425	11.487	10.361	8.768	9.3*
Ta	BCC	187.810	181.116	205.534	199.998	196.462	163.345	212.634	209.379	232.166	210.435	218.981	198.963	200.0
W	BCC	286.450	267.864	318.164	306.480	301.692	296.696	329.641	326.147	357.702	325.181	340.697	309.646	323.2
Ir	FCC	301.726	259.177	359.776	336.899	329.294	455.665	373.098	370.375	365.836	355.695	398.543	344.228	355.0
Pt	FCC	205.013	171.114	263.095	242.600	232.858	341.923	276.529	273.512	267.401	257.178	302.235	244.982	278.3
Au	FCC	106.016	89.683	155.099	139.849	129.370	191.343	148.255	159.795	156.150	146.611	189.275	136.817	173.2
Pb	FCC	34.303	31.164	44.442	41.991	39.015	25.185	42.843	44.497	41.383	40.978	52.294	39.735	46.8*

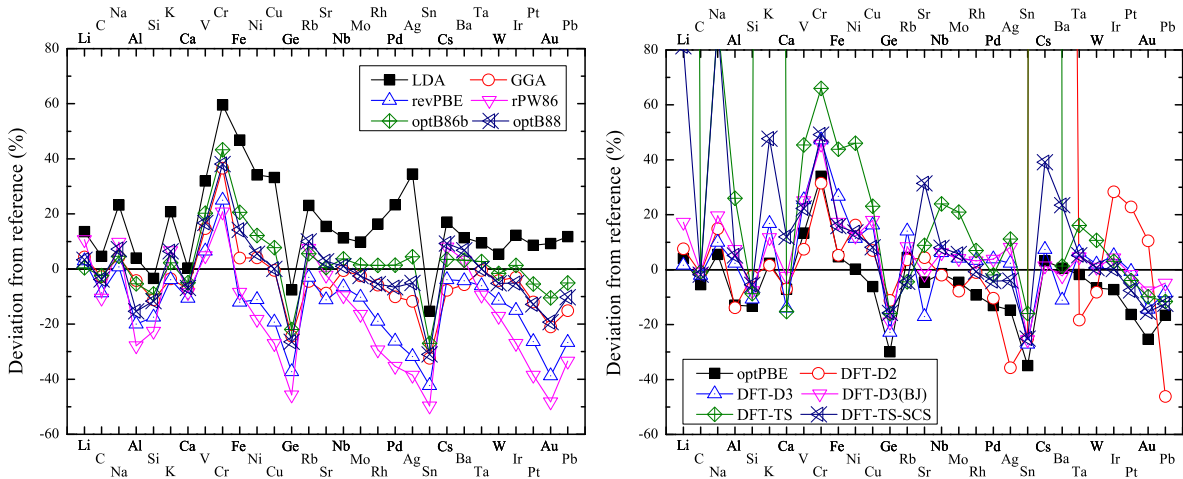


Figure 3: Relative errors in the calculated bulk moduli with respect to the experimental values. Results are shown for the ten vdW functionals and the standard DFT functionals of LDA and GGA. The positive (negative) values in the relative errors represent the larger (smaller) bulk moduli than the experimental values.

Next we discuss the differences among the five vdW results of optB86b-vdW, optB88-vdW, optPBE, DFT-D3, and DFT-D3(BJ). In the case of the DFT-D3 and DFT-D3(BJ) functionals, as expected from the calculated equilibrium lattice constants, the DFT-D3 functional shows either comparable or better results than the DFT-D3(BJ) functional (see

Fig. 4). Better performance of DFT-D3 is observed for alkali and alkali-earth metals. In the case of the optB86b-vdW, optB88-vdW, and optPBE-vdW, the calculated results show very similar behavior, and the optB86b-vdW functional performs better for elements with large atomic number (see Fig. 4).

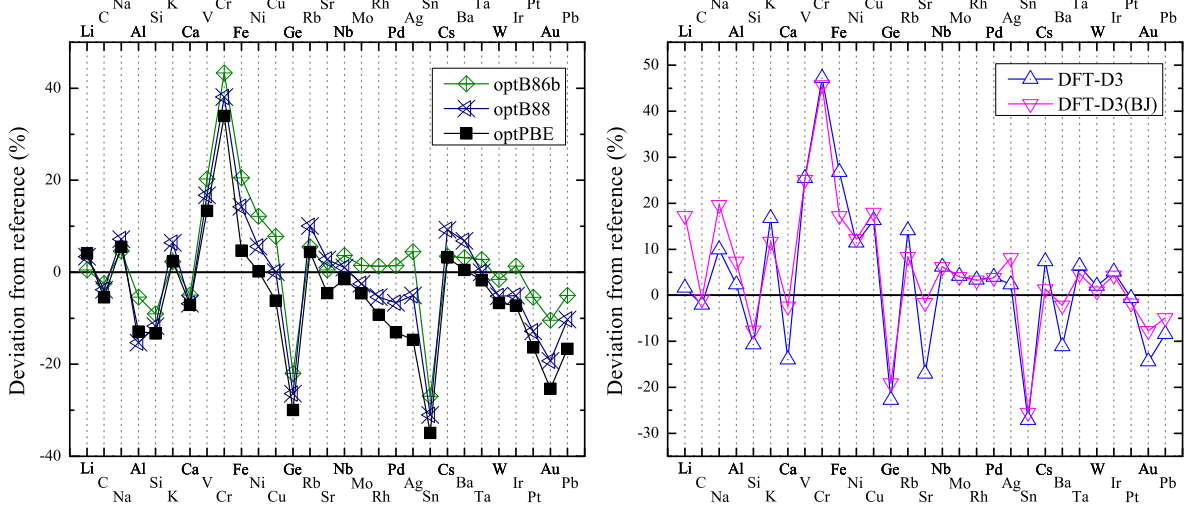


Figure 4: Comparison of the relative errors in the calculated bulk moduli with respect to the experimental values.

3.3. Cohesive energy

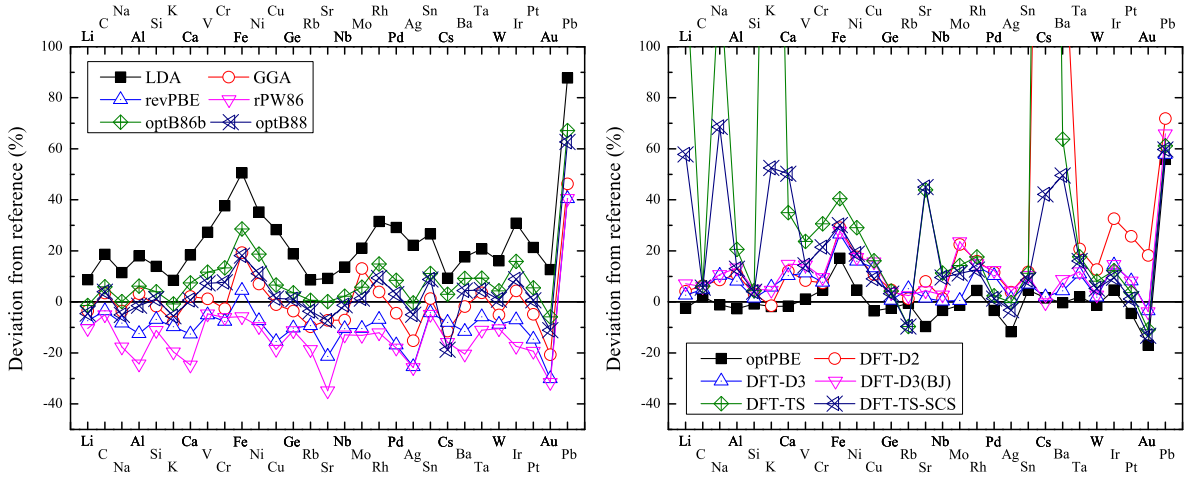


Figure 5: Relative errors in the calculated cohesive energies with respect to the experimental values. Results are shown for the ten vdW functionals and the standard DFT functionals of LDA and GGA. The positive (negative) values in the relative errors represent the larger (smaller) cohesive energies than the experimental values.

The cohesive energies calculated with the ten vdW functionals are summarized in Table 3, and the relative errors in the cohesive energies with respect to the experimental values are presented in Fig. 5. The cohesive energies E_{coh} are calculated using the following equation:

$$E_{\text{coh}} = (E_{\text{tot}} - nE_{\text{atom}})/n, \quad (2)$$

Table 3: Cohesive energies (in eV/atom) for bulk solids with BCC, FCC, and DIA crystal structures using the ten vdW functionals. In addition, standard DFT calculation results using the LDA and the GGA are also shown. The theoretical values are compared to the experimental values. All the experimental cohesive energies [36] were corrected by the zero-point vibration energy E_{ZPV} calculated using the Debye temperature [37].

Solid	Crystal structure	revPBE vdW	rPW86 vdW2	optB86b vdW	optB88 vdW	optPBE vdW	DFT D2	DFT D3	DFT D3(BJ)	DFT TS	DFT TS-SCS	PAW LDA	PAW GGA	Expt.
Li	BCC	1.540	1.490	1.640	1.586	1.622	1.732	1.707	1.782	3.873	2.625	1.808	1.605	1.663
C	DIA	7.323	7.208	8.034	7.891	7.732	8.065	7.959	8.043	8.053	8.012	8.998	7.851	7.586
Na	BCC	1.035	0.929	1.130	1.070	1.115	1.225	1.246	1.249	2.576	1.902	1.258	1.088	1.128
Al	FCC	3.004	2.596	3.643	3.379	3.339	3.800	3.709	3.888	4.137	3.879	4.052	3.544	3.431
Si	DIA	4.369	4.167	4.878	4.744	4.656	4.839	4.761	4.926	4.899	4.880	5.344	4.614	4.693
K	BCC	0.851	0.758	0.935	0.890	0.926	0.929	0.997	0.986	4.196	1.438	1.022	0.869	0.943
Ca	FCC	1.627	1.402	2.001	1.875	1.832	2.086	2.054	2.137	2.514	2.798	2.204	1.903	1.862
V	BCC	5.075	5.094	5.969	5.736	5.407	5.795	5.954	6.123	6.613	6.113	6.809	5.413	5.347
Cr	BCC	3.845	3.906	4.717	4.483	4.355	4.471	4.482	4.559	5.436	5.054	5.728	4.050	4.161
Fe	BCC	4.521	4.074	5.560	5.111	5.065	5.585	5.474	5.524	6.075	5.628	6.511	5.161	4.326
Ni	FCC	4.154	4.050	5.324	4.978	4.691	5.275	5.199	5.268	5.788	5.332	6.063	4.797	4.484
Cu	FCC	2.975	2.868	3.755	3.572	3.399	3.901	3.994	4.075	4.092	3.840	4.521	3.485	3.523
Ge	DIA	3.483	3.444	4.018	3.921	3.787	4.061	3.906	4.025	4.047	4.006	4.611	3.742	3.881
Rb	BCC	0.778	0.698	0.862	0.826	0.853	0.868	0.902	0.879	0.775	0.775	0.931	0.774	0.857
Sr	FCC	1.364	1.130	1.736	1.607	1.566	1.873	1.759	1.810	2.495	2.515	1.894	1.609	1.734
Nb	BCC	6.797	6.613	7.767	7.494	7.345	7.697	7.617	7.804	8.458	8.322	8.636	7.056	7.597
Mo	BCC	6.148	5.966	7.257	6.954	6.770	8.411	6.900	8.487	7.845	7.630	8.310	7.763	6.864
Rh	FCC	5.400	5.093	6.657	6.341	6.057	6.720	6.598	6.667	6.818	6.528	7.622	6.021	5.797
Pd	FCC	3.254	3.209	4.248	4.038	3.785	4.371	4.319	4.399	4.009	3.967	5.058	3.743	3.917
Ag	FCC	2.216	2.206	2.960	2.821	2.625	3.084	3.008	3.098	2.966	2.876	3.631	2.519	2.972
Sn	DIA	3.025	3.007	3.512	3.437	3.307	3.529	3.378	3.488	3.515	3.428	4.001	3.199	3.159
Cs	BCC	0.743	0.679	0.832	0.656	0.820	4.009	0.824	0.805	5.375	1.148	0.883	0.715	0.808
Ba	BCC	1.689	1.520	2.087	1.995	1.904	4.881	1.994	2.079	3.130	2.858	2.248	1.876	1.911
Ta	BCC	7.645	7.220	8.878	8.499	8.285	9.809	9.008	9.080	9.562	9.424	9.807	8.411	8.123
W	BCC	8.152	8.002	9.322	9.013	8.822	10.067	9.107	9.182	9.662	9.412	10.381	8.483	8.939
Ir	FCC	6.489	5.767	8.091	7.602	7.309	9.257	7.990	8.006	7.838	7.639	9.132	7.282	6.981
Pt	FCC	5.006	4.729	6.185	5.900	5.597	7.373	6.342	6.342	6.078	5.929	7.112	5.578	5.863
Au	FCC	2.673	2.619	3.601	3.403	3.175	4.523	3.691	3.679	3.408	3.319	4.309	3.035	3.826
Pb	FCC	2.866	2.868	3.410	3.319	3.180	3.507	3.219	3.384	3.288	3.259	3.831	2.984	2.040

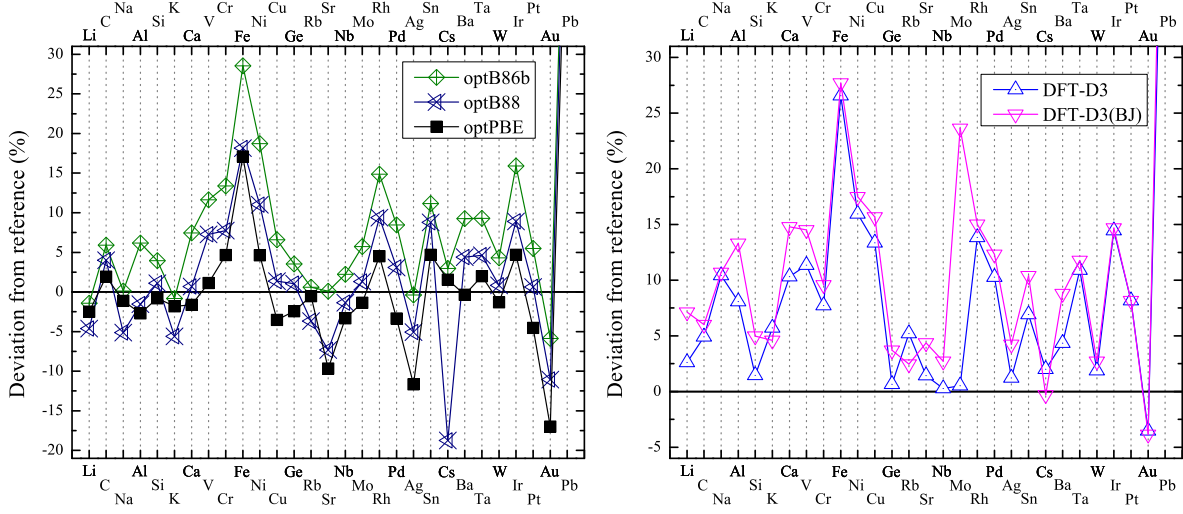


Figure 6: Comparison of the relative errors in the calculated cohesive energies with respect to the experimental values.

where E_{tot} and E_{atom} are the total energy of the system for atoms in the primitive unit cell at equilibrium and an isolated (free) spin-polarized atom, respectively, and n is the number of atoms in the primitive unit cell. The experimental cohesive energies were corrected by the zero-point vibration energy E_{ZPV} calculated using the Debye temperature Θ_D , $E_{\text{ZPV}} = (9/8)k_B\Theta_D$ [37].

For Pb, the relative errors in the calculated cohesive energies are as large as over 40% for all the vdW functionals. In the case of the DFT-TS and DFT-TS-SCS functionals, poor performance is observed for alkali metals (Li, Na, K, Cs). The DFT-D2 functional shows poor performance for Cs and Ba. In the case of the vdW-DF functionals, the revPBE-vdW and rPW86-vdW2 functionals give lower cohesive energies than the other vdW-DF functionals.

Next we discuss the differences among the five vdW results of optB86b-vdW, optB88-vdW, optPBE, DFT-D3, and DFT-D3(BJ). The DFT-D3 functional shows either comparable or better performance compared to the DFT-D3(BJ) (see Fig. 6). In the case of the vdW-DF functionals, the optB86b-vdW, optB88-vdW, and optPBE-vdW functionals show very similar results, although the optB86b-vdW functional gives higher cohesive energies than the optB88-vdW and optPBE-vdW functionals (see Fig. 6).

4. Summary

In summary, we have investigated the lattice constants, the bulk moduli, and the cohesive energies for the bulk solids of 29 elements at equilibrium, using various vdW functionals based on the DFT in the VASP code. The assessed vdW functionals are classified into two groups. One is the vdW-DF functionals made by a proper choice of exchange functional, and the other is the vdW functionals of a dispersion-corrected DFT-D approach in which an atom-pairwise potential is added to a standard DFT result. The DFT-TS and DFT-TS-SCS functionals showed relatively poor performance for alkali and alkali-earth metals. Note that in the case of the DFT-TS and DFT-TS-SCS functionals, effective atomic volumes are used to calculate the dispersion coefficients. For the calculations, the partitioning of the electron density for each atom in a molecule or solid is performed and its result is then used to scale the dispersion coefficient with reference to the corresponding value for a free atom. Our calculations suggest that the partitioning of the electron density for effective atomic volumes may not be sufficiently accurate for delocalized alkali and alkali-earth metals. We obtained a general trend that the vdW functionals (optB86b-vdW, optB88-vdW, and optPBE-vdW) with optimized exchange functionals and the DFT-D vdW functionals [DFT-D3 and DFT-D3(BJ)] give better results than the original revPBE-vdW and rPW86-vdW2 functionals. To further aid in our understanding, we also discussed the differences among the vdW results of optB86b-vdW, optB88-vdW, optPBE-vdW, DFT-D3, and DFT-D3(BJ). These five vdW functionals showed very similar results. The DFT-D3 functional with zero damping gave either comparable

or better performance compared to the DFT-D3(BJ) with damping. In the case of the vdW functionals with optimized exchange functionals, the optB86b-vdW showed slightly better performance in the equilibrium lattice constants and the bulk moduli compared to the other vdW functionals of optB88-vdW and optPBE-vdW. For the cohesive energies, the vdW functionals of optB86b-vdW, optB88-vdW, and optPBE-vdW functionals showed very similar results with smaller variation compared to the original vdW-DF methods of revPBE-vdW and rPW86-vdW2 and the standard LDA method. The results we present in this study provide fundamental information on how the various vdW functionals perform for the selected solid elements, including alkali, alkali-earth, and transition metals, with BCC, FCC, and diamond structures as the ground state structure.

5. Acknowledgments

This research was supported by Nano Material Technology Development Program (2012M3A7B4049888) through the National Research Foundation of Korea (NRF) funded by the Ministry of Science, ICT and Future Planning (MSIP), and Priority Research Center Program (2010-0020207) through NRF funded by the Ministry of Education (MOE). Calculations were performed by using the supercomputing resources (KSC-2014-C1-002) of the Korea Institute of Science and Technology Information (KISTI) and Korea Research Environment Open NETwork (KREONET), and the Partnership & Leadership for the nationwide Supercomputing Infrastructure (PLSI).

References

- [1] P. Hohenberg, W. Kohn, Inhomogeneous electron gas, *Phys. Rev.* 136 (1964) B864–B871. doi:[10.1103/PhysRev.136.B864](https://doi.org/10.1103/PhysRev.136.B864).
- [2] W. Kohn, L. J. Sham, Self-consistent equations including exchange and correlation effects, *Phys. Rev.* 140 (1965) A1133–A1138. doi:[10.1103/PhysRev.140.A1133](https://doi.org/10.1103/PhysRev.140.A1133).
- [3] S. V. Aradhya, M. Frei, M. S. Hybertsen, L. Venkataraman, Van der waals interactions at metal/organic interfaces at the single-molecule level, *Nature Mater.* 11 (2012) 872–876. doi:[10.1038/nmat3403](https://doi.org/10.1038/nmat3403).
- [4] T. Björkman, Testing several recent van der waals density functionals for layered structures, *J. Chem. Phys.* 141 (2014) 074708. doi:[10.1063/1.4893329](https://doi.org/10.1063/1.4893329).
- [5] T. Bučko, J. Hafner, S. Lebègue, J. G. Ángyán, Improved description of the structure of molecular and layered crystals: Ab initio dft calculations with van der waals corrections, *J. Phys. Chem. A* 114 (43) (2010) 11814–11824. doi:[10.1021/jp106469x](https://doi.org/10.1021/jp106469x).
- [6] J. Park, B. D. Yu, S. Hong, Ab initio calculations with van der waals corrections: Benzene-benzene intermolecular case and graphite, *J. Korean Phys. Soc.* 59 (2011) 196–199. doi:[10.3938/jkps.59.196](https://doi.org/10.3938/jkps.59.196).
- [7] H. Kim, Effect of van der waals interaction on the structural and cohesive properties of black phosphorus, *J. Korean Phys. Soc.* 64 (2014) 547–553. doi:[10.3938/jkps.64.547](https://doi.org/10.3938/jkps.64.547).
- [8] L. Schimka, R. Gaudoin, J. Klimeš, M. Marsman, G. Kresse, Lattice constants and cohesive energies of alkali, alkaline-earth, and transition metals: Random phase approximation and density functional theory results, *Phys. Rev. B* 87 (2013) 214102. doi:[10.1103/PhysRevB.87.214102](https://doi.org/10.1103/PhysRevB.87.214102).
- [9] P. Haas, F. Tran, P. Blaha, Calculation of the lattice constant of solids with semilocal functionals, *Phys. Rev. B* 79 (2009) 085104. doi:[10.1103/PhysRevB.79.085104](https://doi.org/10.1103/PhysRevB.79.085104).
- [10] M. Dion, H. Rydberg, E. Schröder, D. C. Langreth, B. I. Lundqvist, Van der waals density functional for general geometries, *Phys. Rev. Lett.* 92 (2004) 246401. doi:[10.1103/PhysRevLett.92.246401](https://doi.org/10.1103/PhysRevLett.92.246401).
- [11] J. Klimeš, A. Michaelides, Perspective: Advances and challenges in treating van der waals dispersion forces in density functional theory, *J. Chem. Phys.* 137 (2012) 120901. doi:[10.1063/1.4754130](https://doi.org/10.1063/1.4754130).
- [12] K. Lee, E. D. Murray, L. Kong, B. I. Lundqvist, D. C. Langreth, Higher-accuracy van der waals density functional, *Phys. Rev. B* 82 (2010) 081101. doi:[10.1103/PhysRevB.82.081101](https://doi.org/10.1103/PhysRevB.82.081101).
- [13] E. D. Murray, K. Lee, D. C. Langreth, Investigation of exchange energy density functional accuracy for interacting molecules, *J. Chem. Theory Comput.* 5 (2009) 2754–2762. doi:[10.1021/ct900365q](https://doi.org/10.1021/ct900365q).
- [14] J. Klimeš, D. R. Bowler, A. Michaelides, Chemical accuracy for the van der waals density functional, *J. Phys.: Condens. Matter* 22 (2010) 022201. doi:[10.1088/0953-8984/22/2/022201](https://doi.org/10.1088/0953-8984/22/2/022201).
- [15] J. Klimeš, D. R. Bowler, A. Michaelides, Van der waals density functionals applied to solids, *Phys. Rev. B* 83 (2011) 195131. doi:[10.1103/PhysRevB.83.195131](https://doi.org/10.1103/PhysRevB.83.195131).
- [16] S. Grimme, Accurate description of van der waals complexes by density functional theory including empirical corrections, *J. Comput. Chem.* 25 (2004) 1463–1473. doi:[10.1002/jcc.20078](https://doi.org/10.1002/jcc.20078).
- [17] S. Grimme, Semiempirical gga-type density functional constructed with a long-range dispersion correction, *J. Comput. Chem.* 27 (2006) 1787–1799. doi:[10.1002/jcc.20495](https://doi.org/10.1002/jcc.20495).
- [18] S. Grimme, J. Antony, S. Ehrlich, H. Krieg, A consistent and accurate ab initio parametrization of density functional dispersion correction (dft-d) for the 94 elements h-pu, *J. Chem. Phys.* 132 (2010) 154104. doi:[10.1063/1.3382344](https://doi.org/10.1063/1.3382344).
- [19] S. Grimme, S. Ehrlich, L. Goerigk, Effect of the damping function in dispersion corrected density functional theory, *J. Comput. Chem.* 32 (2011) 1456–1465. doi:[10.1002/jcc.21759](https://doi.org/10.1002/jcc.21759).
- [20] A. Tkatchenko, M. Scheffler, Accurate molecular van der waals interactions from ground-state electron density and free-atom reference data, *Phys. Rev. Lett.* 102 (2009) 073005. doi:[10.1103/PhysRevLett.102.073005](https://doi.org/10.1103/PhysRevLett.102.073005).

- [21] A. Tkatchenko, R. A. DiStasio, R. Car, M. Scheffler, Accurate and efficient method for many-body van der waals interactions, *Phys. Rev. Lett.* 108 (2012) 236402. doi:[10.1103/PhysRevLett.108.236402](https://doi.org/10.1103/PhysRevLett.108.236402).
- [22] T. Bučko, S. Lebègue, J. Hafner, J. G. Ángyán, Tkatchenko-scheffler van der waals correction method with and without self-consistent screening applied to solids, *Phys. Rev. B* 87 (2013) 064110. doi:[10.1103/PhysRevB.87.064110](https://doi.org/10.1103/PhysRevB.87.064110).
- [23] G. Kresse, J. Hafner, *Ab initio* molecular dynamics for liquid metals, *Phys. Rev. B* 47 (1993) 558. doi:[10.1103/PhysRevB.47.558](https://doi.org/10.1103/PhysRevB.47.558).
- [24] G. Kresse, J. Hafner, *Ab initio* molecular-dynamics simulation of the liquid-metal amorphous-semiconductor transition in germanium, *Phys. Rev. B* 49 (1994) 14251–14269. doi:[10.1103/PhysRevB.49.14251](https://doi.org/10.1103/PhysRevB.49.14251).
- [25] G. Kresse, J. Furthmüller, Efficient iterative schemes for *ab initio* total-energy calculations using a plane-wave basis set, *Phys. Rev. B* 54 (1996) 11169–11186. doi:[10.1103/PhysRevB.54.11169](https://doi.org/10.1103/PhysRevB.54.11169).
- [26] G. Kresse, J. Furthmüller, Efficiency of ab-initio total energy calculations for metals and semiconductors using a plane-wave basis set, *Comput. Mater. Sci.* 6 (1996) 15–50. doi:[10.1016/0927-0256\(96\)00008-0](https://doi.org/10.1016/0927-0256(96)00008-0).
- [27] D. M. Ceperley, B. J. Alder, Ground state of the electron gas by a stochastic method, *Phys. Rev. Lett.* 45 (1980) 566–569. doi:[10.1103/PhysRevLett.45.566](https://doi.org/10.1103/PhysRevLett.45.566).
- [28] J. P. Perdew, K. Burke, M. Ernzerhof, Generalized gradient approximation made simple, *Phys. Rev. Lett.* 77 (1996) 3865–3868. doi:[10.1103/PhysRevLett.77.3865](https://doi.org/10.1103/PhysRevLett.77.3865).
- [29] P. E. Blöchl, Projector augmented-wave method, *Phys. Rev. B* 50 (1994) 17953–17979. doi:[10.1103/PhysRevB.50.17953](https://doi.org/10.1103/PhysRevB.50.17953).
- [30] G. Kresse, D. Joubert, From ultrasoft pseudopotentials to the projector augmented-wave method, *Phys. Rev. B* 59 (1999) 1758–1775. doi:[10.1103/PhysRevB.59.1758](https://doi.org/10.1103/PhysRevB.59.1758).
- [31] J. Paier, M. Marsman, K. Hummer, G. Kresse, I. C. Gerber, J. G. Ángyán, Screened hybrid density functionals applied to solids, *J. Chem. Phys.* 124 (15) (2006) 154709. doi:[10.1063/1.2187006](https://doi.org/10.1063/1.2187006).
- [32] P. E. Blöchl, O. Jepsen, O. K. Andersen, Improved tetrahedron method for brillouin-zone integrations, *Phys. Rev. B* 49 (1994) 16223–16233. doi:[10.1103/PhysRevB.49.16223](https://doi.org/10.1103/PhysRevB.49.16223).
- [33] F. Birch, Finite elastic strain of cubic crystals, *Phys. Rev.* 71 (1947) 809–824. doi:[10.1103/PhysRev.71.809](https://doi.org/10.1103/PhysRev.71.809).
- [34] Y.-R. Jang, B. D. Yu, Structural, magnetic, and electronic properties of fe, *J. Magn.* 16 (2011) 201–205. doi:[10.4283/JMAG.2011.16.3.201](https://doi.org/10.4283/JMAG.2011.16.3.201).
- [35] Y.-R. Jang, B. D. Yu, Hybrid functional study of the structural and electronic properties of co and ni, *J. Phys. Soc. Jpn.* 81 (2012) 114715. doi:[10.1143/JPSJ.81.114715](https://doi.org/10.1143/JPSJ.81.114715).
- [36] C. Kittel, *Introduction to Solid State Physics*, 8th Edition, Wiley, 2004.
- [37] G. I. Csonka, J. P. Perdew, A. Ruzsinszky, P. H. T. Philipsen, S. Lebègue, J. Paier, O. A. Vydrov, J. G. Ángyán, Assessing the performance of recent density functionals for bulk solids, *Phys. Rev. B* 79 (2009) 155107. doi:[10.1103/PhysRevB.79.155107](https://doi.org/10.1103/PhysRevB.79.155107).
- [38] M. Fuchs, M. Bockstedte, E. Pehlke, M. Scheffler, Pseudopotential study of binding properties of solids within generalized gradient approximations: The role of core-valence exchange correlation, *Phys. Rev. B* 57 (1998) 2134–2145. doi:[10.1103/PhysRevB.57.2134](https://doi.org/10.1103/PhysRevB.57.2134).
- [39] A. van de Walle, G. Ceder, Correcting overbinding in local-density-approximation calculations, *Phys. Rev. B* 59 (1999) 14992–15001. doi:[10.1103/PhysRevB.59.14992](https://doi.org/10.1103/PhysRevB.59.14992).